Compound parabolic concentrators for narrowband wireless infrared receivers

Keang-Po Ho
Joseph M. Kahn
University of California at Berkeley
Department of Electrical Engineering and Computer Sciences
514 Cory Hall
Berkeley, California 94720
E-mail: kpho@eecs.berkeley.edu

Abstract. We discuss the design of optical concentrators based on dielectric and hollow compound parabolic concentrators (CPCs), for use in free-space infrared communication receivers. In order to acheive a high signal-to-noise ratio in a direct-detection receiver, it is desirable to use an optical bandpass filter that passes the signal but attenuates ambient radiation. Placement of a planar bandpass filter at the entrance aperture of a CPC results in a receiver having a narrow passband and high gain, but a narrow acceptance angle. The addition of a second, angle-transforming CPC at the entrance aperture allows the receiver to achieve simultaneously a narrow passband and an acceptance angle approaching 90 deg. We have employed a Monte Carlo ray tracing method to calculate the optical gains of several optical concentrator designs. We find that the optical gains of single and double CPCs are, respectively, about 94% and 93% those of ideal optical concentrators, while addition of planar bandpass filters decreases these gains to about 88% and 86%, respectively. We compare the performance and size of CPC-based concentrators with those based on dielectric hemispheres fitted with hemispherical bandpass filters.

Subject terms: compound parabolic concentrators (CPCs); optical bandpass filters; Monte Carlo ray tracing; wireless infrared communications.

Optical Engineering 34(5), 1385–1395 (May 1995).

1 Introduction

The desire for inexpensive, high-speed wireless links has motivated recent interest in infrared free-space communication systems.[1–5] As a medium for short-range wireless communication, infrared offers significant advantages over radio. The infrared spectrum represents an immense, unregulated bandwidth. Moreover, infrared radiation does not pass through walls, allowing the operation of at least one infrared link in every room of a building without interference. When an infrared link employs intensity modulation with direct detection (IM/DD), the short carrier wavelength and large square-law detector lead to efficient spatial diversity that prevents multipath fading.[5] By contrast, radio links are typically subject to large fluctuations in received signal magnitude and phase.

However, the infrared medium is not without drawbacks. In many indoor environments there exists an intense infrared ambient radiation, arising from sunlight, incandescent lighting, and fluorescent lighting, which induces noise in an infrared receiver. In many systems, it is desirable to employ nondirectional transmitters and receivers, alleviating the need for alignment between them, but this leads to a high path loss. For most applications, IM/DD is the only practical transmission technique. Unfortunately, the electrical signal-to-noise ratio (SNR) of a DD receiver is proportional to the square of the received optical power, implying that IM/DD infrared links require a high transmitter power and can tolerate only a small path loss. While the transmitter power level can usually be increased without fear of interfering with other users, transmitter power may be limited by concerns of power consumption and eye safety, particularly in portable transmitters.

The effects of ambient infrared radiation and path loss can be mitigated by design of receivers having narrow optical bandwidth and large effective collection area. Use of a transmitter having a narrow optical spectrum, such as a single- or nearly single-frequency laser diode, allows the receiver to employ a narrowband optical filter to reject out-of-band ambient light. While the effect of path loss can be overcome by using a large detector area, the accompanying high capacitance leads to a reduction of receiver bandwidth and an increase of receiver thermal noise.[4] Therefore, it is desirable to employ an optical concentrator to increase the effective collection area of the receiver. Previous works[4–7] have analyzed and optimized the design of omnidirectional receivers using hemispherical dielectric concentrators in conjunction with multilayer bandpass filters deposited or bonded onto the hemispherical surface to screen out unwanted ambient radiation (see Fig. 1). Both in systems where the signal radia-

Paper 06114 received Nov. 5, 1994; revised manuscript received Dec. 9, 1994; accepted for publication Dec. 9, 1994.
© 1995 Society of Photo-Optical Instrumentation Engineers. 0091-3286/95/$6.00.

Downloaded from SPIE Digital Library on 29 Sep 2010 to 171.64.84.32. Terms of Use: http://spiedl.org/terms

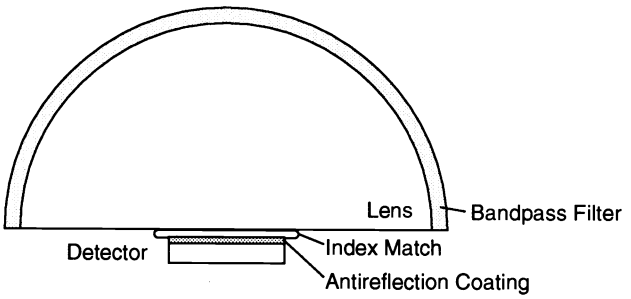

Fig. 1 Cross-sectional view of a receiver structure that achieves optical gain, wide FOV, and narrow passband. The hemispherical concentrator of refractive index N provides a nearly omnidirectional optical gain of approximately N^2, as long as its radius is sufficiently large compared to the detector radius. (From Refs. 4, 6.)

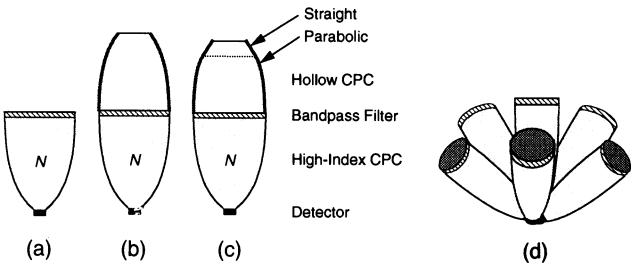

Fig. 2 Receiver structures combining CPCs with bandpass optical filters to achieve different acceptance angles: (a) single dielectric CPC, yielding small acceptance angle; (b) dielectric CPC combined with parabolic hollow CPC, achieving an acceptance angle of 90 deg; (c) dielectric CPC combined with hollow CPC having a straight section, achieving an acceptance angle less than 90 deg; (d) array of directional elements oriented in different directions.

tion is received from a single direction[4–6] (line-of-sight systems) and in systems where the received signal radiation is approximately isotropic[7] (diffuse systems), the power coupled to the detector can be increased by a factor of N^2, as long as the hemisphere is sufficiently large compared to the detector. The concentration ratio of N^2 is actually the thermodynamic limit of a concentrator for isotropic, diffuse radiation.[8] When the hemisphere is sufficiently large, all rays reaching the detector strike the hemispherical optical filter at near-normal incidence, allowing the use of a narrow filter bandwidth without restricting the receiver field of view (FOV). However, it may be difficult to manufacture a hemispherical filter, particularly one that has a narrow passband, which requires that the filter center wavelength must be controlled very accurately.

Another means of nearly approaching the thermodynamic limit of optical concentration is to use rotationally symmetric, three-dimensional compound parabolic concentrators (CPCs).[3–10] Receiving elements using CPCs promise several advantages over those based on hemispheres. CPC-based receivers can be designed to achieve any FOV between nearly 0 and 90 deg, and when the FOV is less than 90 deg, the thermodynamic-limited signal gain can exceed N^2, reducing the required detector area. Also, CPC-based concentrators utilize flat optical bandpass filters, which can be fabricated easily using standard techniques. The bandpass of a flat filter can be tuned by tilting the filter, which may permit the center-wavelength manufacturing tolerances to be relaxed.

Figure 2 shows four different types of receivers, suitable for different applications, which combine CPC-based concentrators with planar bandpass filters. The receiver of Fig. 2(a) is suitable for applications requiring a narrow receiver FOV; the receiver FOV is equal to either the angular bandwidth of the bandpass filter or the acceptance angle of the CPC, whichever is smaller. Figure 2(b)–2(d) represents receivers that achieve much wider FOVs. In the design of Fig. 2(b), a second, hollow CPC is placed on top of the concentrator of Fig. 2(a). This inverted CPC accepts radiation from a FOV of 90 deg and transfers it to angles that lie within the FOV of the lower-filter–CPC combination. Modification of the upper CPC by addition of a straight section results in the design of Fig. 2(c), which can achieve any desired receiver FOV intermediate between 90 deg and the FOV of the lower-filter–CPC combination. In the concentrators of Fig. 2(a) and 2(b), the upper CPC can be either hollow or dielectric filled, but use of a hollow upper CPC will reduce the overall length of the concentrator (see Sec. 4). As shown in Fig. 2(d), a wide FOV may also be achieved by use of several elements having narrow FOVs [e.g., those of Fig. 2(a)], which are oriented in different directions.

The single-CPC structure of Fig. 2(a) has been used in a wireless infrared receiver,[3] but not in combination with a bandpass filter. The receiver structures shown in Fig. 2(a)–2(b) have been proposed previously for detection of narrowband radiation.[11,12] An array of CPCs oriented in different directions, similar to Fig. 2(d), has been utilized to achieve coverage of a wide FOV.[13] To our knowledge, however, the systematic design of these structures has not been addressed, either analytically or numerically. In this paper, we study the design of the structures shown in Fig. 2(a)–2(c) using both analytical and numerical techniques. The concentrator of Fig. 2(d), which is a variation on the structure of Fig. 2(a), is not analyzed separately here.

This paper is organized as follows. Section 2 discusses the properties of optical concentrators and bandpass filters. Section 3 describes the Monte Carlo ray tracing used to evaluate the concentrator structures shown in Fig. 2. Section 4 presents a comparison of CPCs and hemispherical concentrators. Our conclusions are presented in Sec. 5.

2 Ideal Concentrators for Narrowband Infrared Receivers

While practical concentrators for wireless infrared receivers are not ideal, in this section we introduce the general features of narrowband concentrator design, making the assumption of ideal concentrators (except in Sec. 2.3). The assumption of concentrator ideality will be relaxed in Sec. 3 below.

2.1 *Properties of Ideal Optical Concentrators*

For an ideal, passive, three-dimensional concentrator, the thermodynamic-limited signal gain, defined to be the maximum achievable increase of irradiance between input and output, is given by[8–10]

$$C=\left(\frac{N\sin\theta_o}{\sin\theta_i}\right)^2, \tag{1}$$

where θ_o and θ_i are the acceptance angles at the output and input apertures, respectively, and $N=n_o/n_i$ is the ratio of

Downloaded from SPIE Digital Library on 29 Sep 2010 to 171.64.84.32. Terms of Use: http://spiedl.org/terms

output and input refractive indices. In what follows, we assume $n_i = 1$, and refer to N simply as the "refractive index."

In a wireless infrared link, the angular distribution of received signal radiation depends on the link design, i.e., source radiation pattern, propagation path, and relative position and orientation of source and receiver. In this paper, we always assume that the desired signal radiation is received with equal power per unit solid angle for all angles within θ_s of some axis (see Fig. 3). Furthermore, we assume that the concentrator has an input acceptance angle or FOV of θ_i, where $\theta_i \le \theta_s$, and that the concentrator is aligned with the central axis of the cone of signal radiation. If we place in the radiation flux a bare detector having area A_d and acceptance angle $\theta_d = 90$ deg, then the total power incident on the detector is proportional to its étendue

$$E_d = \pi A_d \sin^2\theta_s \ . \tag{2}$$

Now suppose that an ideal concentrator is used to concentrate the radiation incident on the detector. Assume that the concentrator input aperture has area A_i, while the concentrator output aperture has area $A_o = A_d$ and acceptance angle $\theta_o = \theta_d = 90$ deg, both matched to the detector. For an ideal concentrator with an acceptance angle of $\theta_i \le \theta_s$, the étendue at both the concentrator input and output apertures is

$$E_i = E_o = \pi A_i \sin^2\theta_i \ . \tag{3}$$

Because $A_i/A_d = C$ and $\theta_o = \theta_d = 90$ deg, the signal gain (i.e., the increase of irradiance between input and output) of an ideal concentrator is

$$G_s^{\text{ideal}} = \frac{E_o}{E_d} = N^2 \csc^2\theta_s \ . \tag{4}$$

This signal gain is independent of θ_i, but depends on θ_s. If the signal radiation is distributed uniformly within a cone of angle θ_s, as long as the acceptance angle of the concentrator is smaller than θ_s, the signal gain will be constant. In other words, a concentrator having a narrow FOV can be employed for wide-angle radiation without loss of signal gain. In Sec. 4, we show that for a given value of θ_s, the length of a CPC-based concentrator is minimized by the choice $\theta_i = \theta_s$. We note that when the incident signal radiation is isotropic, i.e., $\theta_s = 90$ deg, then the gain of an ideal concentrator is $G_s^{\text{ideal}} = N^2$, which is identical to the thermodynamic-limited gain of a hemispherical lens in isotropic radiation.[4–8]

For a given choice of N and θ_s, the gain of a real concentrator, G_s, cannot exceed the gain of an ideal concentrator, i.e., $G_s \le G_s^{\text{ideal}}$. It is shown in Sec. 3 that real concentrators can achieve gains within a few percent of those given by Eq. (4).

2.2 *Multilayer Bandpass Filters*

In a wireless infrared communication system, an optical bandpass filter can be used to limit the ambient radiation reaching the detector. A common form of bandpass filter consists of a stack of dielectric thin-film layers. By properly choosing the number of layers, their thicknesses, and their refractive indices, it is possible to control the surface reflectance and thus the filter transmittance.[14] Multilayer bandpass filters are designed to have a transmittance versus wavelength that is

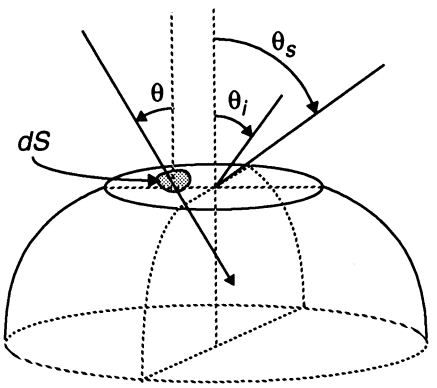

Fig. 3 Input aperture of an optical concentrator. The input signal radiation is distributed with uniform power per unit solid angle over a cone of angle of θ_s. The concentrator has an acceptance angle $\theta_i \le \theta_s$.

peaked at a particular wavelength for a certain angle of incidence, and this peak wavelength shifts with angle of incidence. (The shift of the peak wavelength depends on the polarization of the incident radiation, but this polarization dependence is insignificant for the small angles of incidence considered here and is neglected in the remainder of this paper.) Therefore, a filter having a narrow bandwidth at a particular angle of incidence will, for a particular wavelength, exhibit a narrow angular response. Analysis shows that if the $\Delta\lambda$ is the half-power bandwidth and λ_c is the center wavelength, then the half-power angular bandwidth is approximately

$$\Delta\theta \approx N^* \left(\frac{2\,\Delta\lambda}{\lambda_c} \right)^{1/2} , \tag{5}$$

where N^* is the effective refractive index of the filter.[4,7,14] It is shown below that the receiver electrical SNR is enhanced by use of a filter having a narrow spectral bandwidth, which might appear to imply that the receiver must also have a narrow FOV. We show, however, that a CPC-based receiver need not have a restricted FOV to achieve a narrow spectral bandwidth.

In what follows, we need to calculate the angle- and wavelength-dependent transmittance of multilayer filters. While the greatest accuracy can be achieved using detailed physical models,[14,15] we assume a Butterworth design that can be described fairly accurately by a simple, five-parameter model. In this model, for radiation of wavelength λ incident on the filter at angle θ, the filter transmittance is given by[4]

$$T_f(\lambda,\theta) = \frac{T_{f0}}{1 + \left(\dfrac{\lambda - \lambda_{\text{pk}}(\theta)}{\Delta\lambda/2} \right)^{2m}} , \tag{6}$$

where T_{f0} is the peak transmittance, $\Delta\lambda$ is the half-power bandwidth, and m is the Butterworth order. Here,

$$\lambda_{\text{pk}}(\theta) = \lambda_{\text{normal}} \left[1 - \left(\frac{n_1}{N^*} \right)^2 \sin^2\theta \right]^{1/2} \tag{7}$$

Downloaded from SPIE Digital Library on 29 Sep 2010 to 171.64.84.32. Terms of Use: http://spiedl.org/terms

is the wavelength of peak transmission for light incident at angle θ, where λ_{normal} is the wavelength of peak transmission for normal incidence. The bandpass filter is thus characterized by five parameters: $\Delta\lambda$, λ_{normal}, m, N^*, and T_{f0}. Figure 4 compares wavelength-dependent transmittance curves calculated for several angles of incidence using both the five-parameter model and a detailed physical model, for a 30-nm-wide bandpass filter similar to one used in an experimental infrared link.[16] Except for the degree of passband smoothness, results of the two models do not differ significantly over the range of angles of incidence considered here.

2.3 *Figure of Merit for a Narrowband Concentrator*

In this section, we derive a figure of merit that is useful for comparing the performance of different narrowband concentrators. We assume that the signal is generated by a source, such as a single- or nearly single-frequency laser, that has a linewidth much smaller than the filter bandwidth. If the received source radiation has an irradiance p_s (power per unit area), the signal power received by the detector is

$$P_s = p_s A_d G_s \bar{T}_s \ , \tag{8}$$

where A_d is the detector area and G_s is the signal gain of the concentrator, which is not generally equal to the ideal-concentrator gain (4). The factor $\bar{T}_s$ is the transmittance of the filter at the signal wavelength, which represents an average of its angle-dependent transmission over different angles of incidence.

We assume here that the optical power spectral density of the ambient radiation is constant over the entire spectral region near the passband of the filter. If this ambient radiation is described by a spectral irradiance p_n (representing power per unit area per unit wavelength), then the total optical noise power received by the detector is

$$P_n = p_n A_d G_n T_{f0} \Delta\lambda_n \ , \tag{9}$$

where T_{f0} and $\Delta\lambda_n$ are, respectively, the peak transmittance and effective noise bandwidth of the filter.[5] The factor G_n represents the optical concentrator gain for ambient radiation, which depends on the ambient's angular distribution. Assuming that the background radiation is isotropic, and making the slightly pessimistic assumption that the concentrator behaves ideally for noise, then $G_n = N^2$, and

$$P_n = p_n A_d N^2 T_{f0} \Delta\lambda_n \ . \tag{10}$$

For a general filter-concentrator combination, the filter effective noise bandwidth $\Delta\lambda_n$ depends on the characteristics of both the filter and the concentrator, especially in that the latter limits the FOV of the combination. In computing $\Delta\lambda_n$ for a real filter, one must consider that the shape of the wavelength-dependent filter transmission curve $T_f(\lambda,\theta)$ depends on the incidence angle θ. This change in shape is most apparent[4,14] at large θ. For example, in Fig. 4 we observe a notable change in the shape of $T_f(\lambda,\theta)$, computed using the theoretical physical model, between θ = 0 and θ = 30 deg. We define an angle-dependent noise bandwidth $\Delta\lambda_n(\theta) = T_{f0}^{-1} \int_\lambda T_f(\lambda,\theta)\, d\lambda$, where the integration is performed over all wavelengths. The overall noise bandwidth can be defined as

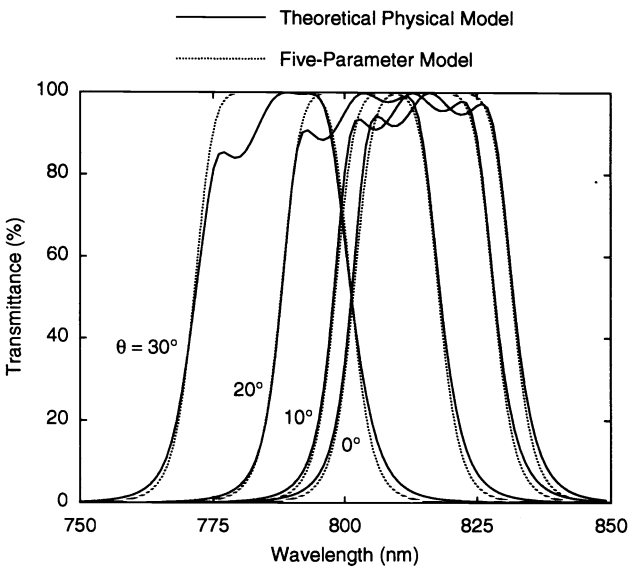

Fig. 4 Theoretical polarization-averaged transmittance versus wavelength for a 29-layer, thin-film optical bandpass filter. At normal incidence, θ = 0 deg, the filter has a half-power bandwidth of 30 nm and a center wavelength of 816.5 nm. The filter is designed with 29 layers arranged $(HL)^2H^4/L(HL)^4H^2L(HL)^4H^2(LH)^2$, in addition to extra layers for index matching and blocking transmission far away from the passband. The indices are $n_H = 2.31$ and $n_L = 1.49$. The transmittance calculated using a five-parameter model (λ_{normal} = 816.5 nm, $\Delta\lambda = 30$ nm, $m = 4$, $N^* = 1.89$, $T_{f0} = 1$) is also shown for comparison.

$$\Delta\lambda_n = \frac{\int_\Omega \Delta\lambda_n(\theta)\, \bar{\tau}_f(\theta) I_f(\theta) \cos\theta \, d\Omega}{\int_\Omega \bar{\tau}_f(\theta) I_f(\theta) \cos\theta \, d\Omega} \ , \tag{11}$$

where $I_f(\theta)$ is the radiosity at the input aperture of the optical filter and $\bar{\tau}_f(\theta)$ is the average (over the filter input aperture) transmittance of radiation from direction θ at the input of filter to the detector. The integration in (11) is performed over all angles. All concentrators considered in this paper are rotationally symmetric, so that both $I_f(\theta)$ and $\bar{\tau}_f(\theta)$ are independent of φ. For all concentrators considered in this paper, both signal and noise passing through the filter to the detector are limited to small angles, i.e., $\bar{\tau}_f(\theta) \to 0$ for large θ. For small incidence angles, the filter transmittance can be accurately modeled by the five-parameter model, in which $\Delta\lambda_n = T_{f0}^{-1} \int_\lambda T_f(\lambda,\theta)\, d\lambda$ is independent of incidence angle θ and is proportional to the half-power bandwidth $\Delta\lambda$. While, in general, $\Delta\lambda_n \neq \Delta\lambda$, for the fourth-order Butterworth filter considered in this paper the difference is very small, i.e., $\Delta\lambda_n \approx 1.025\, \Delta\lambda$. In the remainder of this paper, we quote values of the half-power bandwidth $\Delta\lambda$, rather than the noise bandwidth $\Delta\lambda_n$.

The electrical power of the detected signal is proportional to P_s^2. Both the desired signal and the filtered ambient light generate shot noise. Even with narrowband filtering, under the brightest ambient illumination that the receiver is designed to operate under, the optical power of the received ambient typically is much stronger than the signal power. Under these high-ambient-lighting conditions, the noise in a well-designed DD receiver[4,5] is dominated by the ambient-

Downloaded from SPIE Digital Library on 29 Sep 2010 to 171.64.84.32. Terms of Use: http://spiedl.org/terms

induced shot noise, which has a white electrical power spectral density proportional to P_n. Therefore, the shot-noise-limited electrical SNR of a DD receiver is proportional to the ratio

$$\frac{P_s^2}{P_n}=\frac{p_s^2 A_d (G_s \bar{T}_s)^2}{p_n N^2 T_{f0}\,\Delta\lambda_n} \quad . \tag{12}$$

We define a figure of merit for a concentrator-filter combination, which is proportional to this electrical SNR:

$$M=\frac{(G_s \bar{T}_s)^2}{N^2 T_{f0}\,\Delta\lambda_n} \quad . \tag{13}$$

2.4 *Combination of Bandpass Filters and Ideal Concentrators*

In this section, we discuss the design of the three concentrators shown in Fig. 2(a)–2(c), under the assumption that the CPCs are ideal concentrators.

The design of Fig. 2(a) is suitable for reception of signal radiation confined to a small angle θ_s. Clearly, the overall filter-concentrator combination should have a FOV that does not exceed θ_s, since a larger FOV would admit more background light, but not more signal. This overall FOV is equal either to the filter angular bandwidth $\Delta\theta$ or to the CPC acceptance angle θ_i, whichever is smaller. It is easily argued that the choice $\Delta\theta=\theta_i\le\theta_s$ provides the best utilization of the CPC and filter. Suppose first that $\Delta\theta<\theta_i\le\theta_s$, and that the overall FOV is limited by $\Delta\theta$. In this case, the small value of $\Delta\theta$ implies an unnecessary reduction of the signal gain G_s, reducing the figure of merit (13). Suppose instead that $\theta_i<\Delta\theta\le\theta_s$, and that the overall FOV is limited by θ_i. In this case, the excessively large value of $\Delta\theta$ implies an unnecessary increase of $\Delta\lambda_n$ [recall that $\Delta\theta$ and $\Delta\lambda$ are related via (5)], decreasing the figure of merit (13). It will be shown in Sec. 4 that for a given value of θ_s, the length of a single-CPC concentrator is minimized by the choice $\theta_i=\theta_s$, implying that the best design choice is $\Delta\theta=\theta_i=\theta_s$.

The designs in Fig. 2(b) and 2(c) are concentrators that have wide FOV but narrow bandwidth. The upper CPC is a $\theta_i\rightarrow\theta_m$ transformer, which transfers the radiation from a large input angle θ_i to a smaller intermediate angle θ_m. The upper CPC can be hollow or dielectric-filled; its refractive index does not affect the overall concentrator gain. It is shown in Sec. 4 that the choice of a hollow upper CPC minimizes the required length, and we assume that choice in all that follows. The lower dielectric CPC is designed to have acceptance angle θ_m (referred to as the "intermediate angle"). The concentrator of Fig. 2(b) is designed with $\theta_i=90$ deg, while that of Fig. 2(c) is designed with $\theta_m<\theta_i<90$ deg. In both Fig. 2(b) and 2(c), the intermediate angle θ_m can be chosen to be as small as desired, permitting use of a filter having arbitrarily small angular acceptance $\Delta\theta$, and allowing achievement of an arbitrarily high figure of merit (13). However, choice of very small θ_m will require the upper and lower CPCs to be extremely long (see Sec. 4 below).

3 Optical Gain of Rotationally Symmetric CPCs

The gain of a practical concentrator using a real CPC and bandpass filter cannot be determined analytically.[9,10] Therefore, in this section, we describe the Monte Carlo ray tracing we have used to determine the signal gain, filter transmission, and figure of merit of the concentrators in Fig. 2(a)–2(c).

3.1 *Monte Carlo Ray Tracing*

Figure 3 shows the input aperture of a general optical concentrator, which may include one or two CPCs and a narrowband optical filter. The étendue reaching the output aperture (i.e., the detector) at incidence angle (θ,ϕ) through a small area dS in the input aperture at position $\mathbf{r}$ is described by the transmittance $\tau(\mathbf{r},\theta)$ via

$$dE_o=\tau(\mathbf{r},\theta)\,\cos\theta\;dS\;d\Omega \quad , \tag{14}$$

where $d\Omega=\sin\theta\,d\theta\,d\phi$. While $\tau(\mathbf{r},\theta)$ depends on $\mathbf{r}$ and θ, the concentrator is assumed to be rotationally symmetric, so that $\tau(\mathbf{r},\theta)$ does not depend on the azimuthal angle ϕ. If we assume that the radiation source is uniformly distributed within a FOV of θ_s, after some algebra we find that the total étendue to the concentrator output aperture is

$$E_o=\pi\int_0^{\theta_s}\sin 2\theta\,d\theta\int_{A_{\text{input}}}\tau(\mathbf{r},\theta)\,dS \quad , \tag{15}$$

where the surface integral is performed over the input aperture. If we define the average angular transmittance for incident angle θ as

$$T(\theta)=\frac{1}{A_d}\int_{A_{\text{input}}}\tau(\mathbf{r},\theta)\,dS \quad , \tag{16}$$

then we can compute the concentrator gain as

$$G_s\bar{T}_s=\frac{A_i}{A_d\sin^2\theta_a}\int_0^{\theta_s}T(\theta)\sin 2\theta\,d\theta \quad . \tag{17}$$

We note that since $\tau(\mathbf{r},\theta)$ and $T(\theta)$ represent the transmittance through the entire concentrator, including the optical filter, Eq. (17) yields the product of signal gain G_s times the angle-averaged filter transmission $\bar{T}_s$. If we modify $\tau(\mathbf{r},\theta)$ and $T(\theta)$ to exclude the effect of the optical filter, then Eq. (17) yields simply G_s.

For most practical concentrators, $\tau(\mathbf{r},\theta)$ cannot be found analytically, making it difficult to perform the integration of Eq. (16). For a given incidence angle θ, we perform the integration by using a numerical Monte Carlo method, i.e., by generating a random integration grid, uniformly distributed over the entire input aperture.[17] A geometrical-optics ray tracing algorithm is used to trace both the direction and the power of each ray until it reaches the output aperture or bounces back to the input aperture. The average irradiance of the light at the output aperture is a good approximation to the integral in Eq. (16).

For a rotationally symmetric concentrator, the radiation reaching the output aperture can be found using $T(\theta)$ even in the case that the input radiation is not uniformly distributed within the FOV angle. For example, if the input radiation is characterized by a certain radiance distribution $I(\theta,\phi)$ or $\bar{I}(\theta)=\int_0^{2\pi}I(\theta,\phi)\,d\phi$, the total irradiance at the output aperture can be calculated as

$$I_s=\frac{A_i}{2}\int_0^{\pi/2}\bar{I}(\theta)T(\theta)\,\sin 2\theta\,d\theta \quad . \tag{18}$$

Downloaded from SPIE Digital Library on 29 Sep 2010 to 171.64.84.32. Terms of Use: http://spiedl.org/terms

For our purposes, the angular transmittance $T(\theta)$ summarizes the relevant characteristics of an optical concentrator.

3.2 *Single-CPC Concentrator Having Narrow FOV*

For a single CPC, such as that shown in Fig. 2(a), the filter angular bandwidth $\Delta\theta$ is chosen to equal the CPC acceptance angle θ_i, so that the overall concentrator FOV is also approximately equal to θ_i. We describe the filter angular transmittance using the five-parameter model described in Sec. 2.2. We assume a signal centered at wavelength λ_0, having a linewidth much narrower than the filter bandwidth. For a CPC having a specific acceptance angle θ_i, we satisfy $\Delta\theta = \theta_i$ by choosing the filter design parameters so that at angles 0 and θ_i, the transmittances given by Eq. (6) are 3 dB smaller than the peak transmittance, i.e.,

$$T_f(0,\lambda_0) = T_f(\theta_i,\lambda_0) = T_{f0}/2 \ . \tag{19}$$

This filter design is summarized in Fig. 5. Without loss of generality, we assume $T_{f0} = 1$; if this is not the case, then all of our results are modified by obvious multiplicative factors.

Figure 6 shows the angular transmittance $T(\theta)$ for a concentrator that consists of a CPC having an acceptance angle $\theta_i = 30$ deg, and the bandpass filter shown in Fig. 4. For the signal wavelength $\lambda_0 = 802.5$ nm, this filter satisfies the design criteria of Eq. (19) as shown in Fig. 5. Both a theoretical physical model and a five-parameter model have been used to model the bandpass filter. In Fig. 6, we see that both models yield nearly the same angular transmittance $T(\theta)$, except for small differences arising from the nonsmooth passband of the real filter, which cannot be characterized using the five-parameter model. Figure 6 indicates that the CPC-filter combination achieves an overall FOV close to 30 deg. Because of the design criteria of Eq. (19), as shown in Fig. 5, the transmittance at 0 deg is approximately equal to 50%, and the transmittance falls well below 100% for incidence angles less than 10 deg.

For the optical concentrator design of Fig. 2(a), Fig. 7 shows the signal gain as a function of the input acceptance angle of the dielectric CPC, assuming a CPC refractive index of 1.7. The input source is assumed to be distributed uniformly over an angle equal to the acceptance angle of the CPC, i.e., $\theta_i = \theta_s$. Figure 7 also shows the signal gain of an ideal concentrator, $G_s^{\text{ideal}} = N^2 \csc^2\theta_s$, for comparison. When no filter is utilized, the gain G_s of the CPC is 94% to 95% of that of the ideal concentrator. This 5% to 6% discrepancy arises because of the nonideal nature of the CPC; reflection losses within the CPC are negligible, since it relies upon total internal reflection at the parabolic surface. Adding an optical filter having $N^* = 1.89$ and $m = 4$ (like the filter in Fig. 4), and satisfying Eq. (19) for a signal wavelength of $\lambda_0 = 800$ nm, the simulated product $G_s\overline{T}_s$ is about 88% to 89% of the ideal-concentrator gain G_s^{ideal}. This indicates that, for single-CPC concentrators, the bandpass filter design criterion

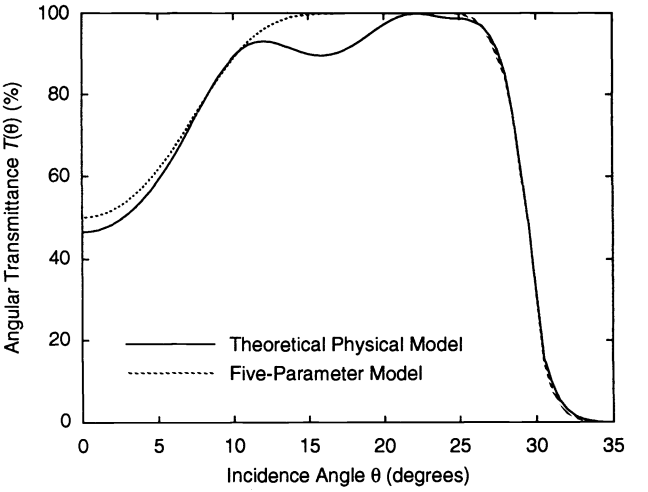

Fig. 6 The angular transmittance $T(\theta)$ of an optical concentrator combining a single CPC with a bandpass filter. Both CPC and filter have acceptance angles of 30 deg. Results of simulations performed using both the theoretical physical model and a five-parameter model for the filter are shown for comparison.

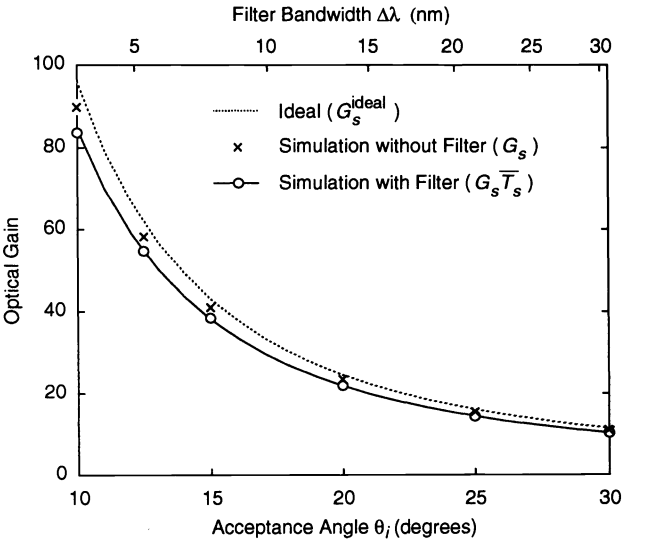

Fig. 7 Optical gain for concentrator combining single CPC and bandpass filter, as a function of concentrator acceptance angle θ_i (and, equivalently, the bandwidth $\Delta\lambda$ of the bandpass filter), comparing simulation results with results assuming an ideal concentrator. The angular bandwidth of the bandpass filter and the acceptance angle of the CPC both equal θ_i. The input source is assumed to be distributed uniformly over an angle equal to the acceptance angle of the CPC, i.e., $\theta_i = \theta_s$.

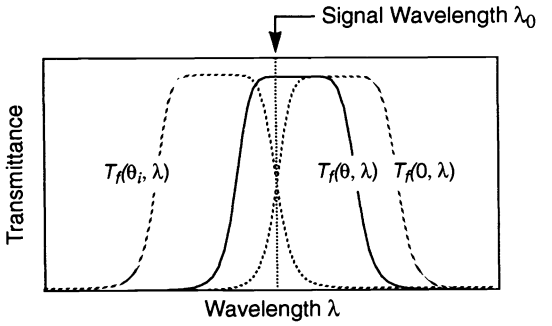

Fig. 5 The optical bandpass filter center wavelength and bandwidth are chosen so that $T_f(0,\lambda_0) = T_f(\theta_i,\lambda_0) = T_{f0}/2$, where T_{f0} is the filter peak transmittance, λ_0 is the signal wavelength, and θ_i is the input angle of acceptance of the dielectric CPC.

Downloaded from SPIE Digital Library on 29 Sep 2010 to 171.64.84.32. Terms of Use: http://spiedl.org/terms

(19) leads to an angle-averaged filter transmission that is fixed at $\overline{T}_s = 94\%$.

3.3 *Double-CPC Concentrator Having 90-deg FOV*

The double CPCs in Fig. 2(b) and 2(c) have FOVs larger than the angular bandwidth of the bandpass filter. The lower CPCs are dielectric, relying upon total internal reflection, which yields a surface reflectance close to 100%. The upper CPCs are hollow, and have internal surfaces coated with reflective coatings, whose reflectance may be somewhat lower than 100%, affecting the angular transmittance $T(\theta)$ of the overall concentrator. Figure 8 shows the $T(\theta)$ calculated for the concentrator in Fig. 2(b) with $\theta_i = 90$ deg and $\theta_m = 20$ deg, for several values of the surface reflectance of the upper hollow CPC. The lower dielectric CPC has a refractive index of 1.7, and the bandpass filter is chosen according to Eq. (19). Simulation shows that the angle-averaged signal gain is reduced by a greater factor than the reflectance of the upper hollow CPC, and that the reduction depends on the value of the intermediate angle θ_m. If the signal gain of the concentrator with 100% reflectance is G_s, empirically we find that the gain with reflectance $\rho < 1$ is approximately $\rho^{\alpha} G_s$, where $\alpha > 1$ can be interpreted as the average number of reflections in the upper hollow CPC. For the CPC described in Fig. 8, Fig. 9 presents α as a function of θ_m. We see that as θ_m increases, α decreases. For example, if $\theta_m = 20$ deg then $\alpha \approx 1.3$, while if $\theta_m = 10$ deg then $\alpha \approx 1.6$.

The gain and figure of merit of double-CPC concentrators are presented in Fig. 10 as a function of the intermediate angle θ_m (and, equivalently, of the spectral bandwidth $\Delta\lambda$). These have been determined under the assumptions that the upper CPC has 100% reflectance, and that the filter transmittance satisfies $T_{f0} = 1$. The lower dielectric CPC is the same as that described in Fig. 7, although it is now described by θ_m instead of θ_i. Simulation indicates that without the bandpass filter in place, the signal gain G_s of the double CPC is 93% to 96% of the ideal-concentrator gain G_s^{ideal}, with the discrepancy arising from the nonideal nature of CPCs. With the bandpass filter in place, simulation shows that for the double CPC, the product $G_s\overline{T}_s$ is 86% to 89% of G_s^{ideal}. This indicates that for these concentrators, the bandpass filter design criterion (19) leads to an angle-averaged filter transmission that is fixed at $\overline{T}_s = 93\%$.

Figure 10 also indicates the gain and figure of merit for an idealized hemispherical-lens–filter combination[4,6] for $N = 1.7$ and for $\Delta\lambda = 5$, 10, and 20 nm. For simplicity, we consider the gain to be N^2 and the figure of merit to be $N^2/\Delta\lambda$, which are upper bounds on the performance of real hemispherical concentrators in isotropic radiation. As an example of the comparison between CPC-based and hemi-

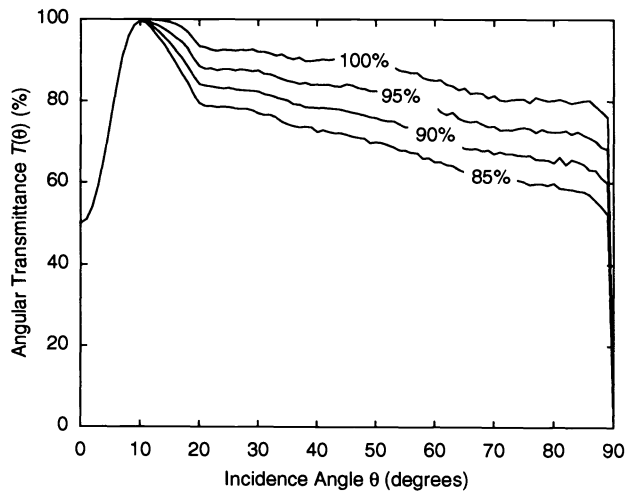

Fig. 8 Angular transmittance $T(\theta)$ for a double CPC having an acceptance angle $\theta_i = 90$ deg. Hollow CPCs having different reflectivities are shown for comparison. The intermediate angle is $\theta_m = 20$ deg.

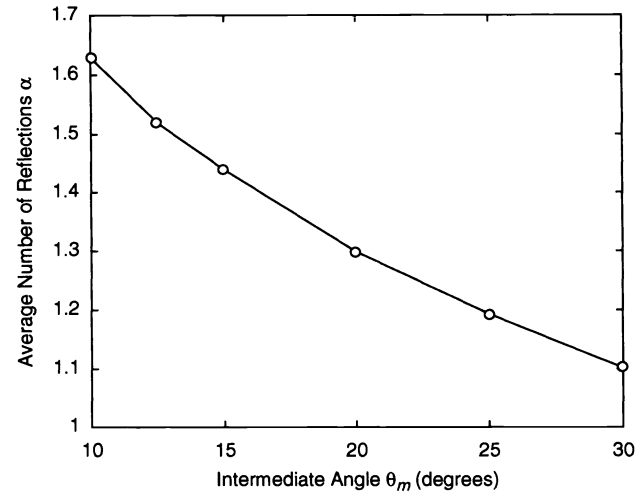

Fig. 9 Average number of reflections within the upper CPC of a double CPC, as a function of the intermediate angle θ_m. The upper CPC has an input acceptance angle $\theta_i = 90$ deg.

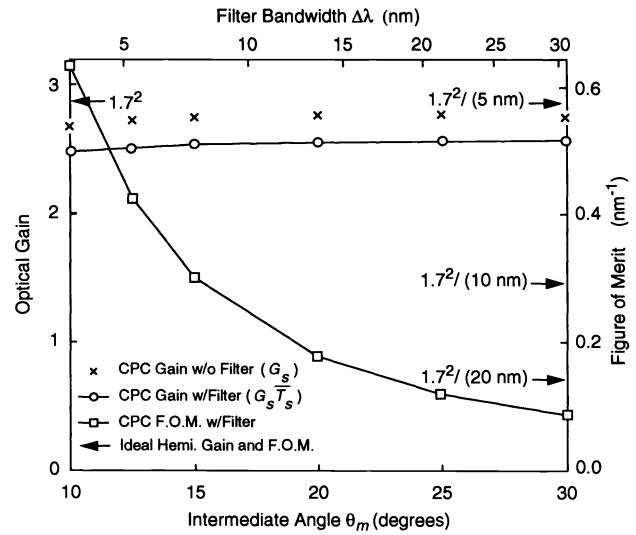

Fig. 10 Optical gain and figure of merit of a double CPC having input acceptance angle $\theta_i = 90$ deg, as a function of the intermediate angle θ_m (and, equivalently, the bandwidth $\Delta\lambda$ of the bandpass filter). The input signal radiation is isotropic. The hollow CPC has a reflectance of 1, and the dielectric CPC has a refractive index of 1.7. Also indicated are the gain N^2 and the figure of merit $N^2/\Delta\lambda$ of an ideal hemispherical filter-concentrator, for $N = 1.7$ and for $\Delta\lambda = 5$, 10, and 20 nm.

Downloaded from SPIE Digital Library on 29 Sep 2010 to 171.64.84.32. Terms of Use: http://spiedl.org/terms

spherical concentrator-filter combinations, consider a hemispherical filter having a bandwidth of 10 nm, which is extremely difficult to fabricate by deposition onto a hemispherical surface. Examination of Fig. 10 shows that the same figure of merit can be achieved using a double CPC with intermediate angle $\theta_m = 15$ deg, which utilizes a flat filter having a bandwidth $\Delta\lambda = 7.5$ nm. Use of a double CPC having a smaller intermediate angle will result in an even higher figure of merit. Planar bandpass filters with bandwidths in the 1- to 5-nm range are fabricated routinely,[14] implying that in practice, a double-CPC concentrator may achieve a figure of merit much higher than a hemispherical lens-filter combination.

3.4 *Double-CPC Concentrator Having FOV Less Than 90 deg*

The optical concentrator shown in Fig. 2(c) can achieve any FOV in the range between the filter angular bandwidth $\Delta\theta$ and 90 deg. Figure 11 presents the gain and figure of merit of a concentrator having an input FOV $\theta_i = 60$ deg, as a function of the intermediate angle θ_m (and, equivalently, of the spectral bandwidth $\Delta\lambda$). The lower dielectric CPC and bandpass filter are designed according to the same criteria as those of Fig. 7 and Fig. 10. The concentrator is assumed to be illuminated by signal radiation distributed uniformly over a cone of angle $\theta_s = 60$ deg. Including the bandpass filter, the simulated product $G_s\overline{T}_s$ is found to be 85% of the ideal-concentrator gain G_s^{ideal}. Comparing the values of G_s and $G_s\overline{T}_s$ in Fig. 10 with those in Fig. 11, we see that the values in Fig. 11 are larger by a factor of approximately $\csc^2(60\text{ deg}) = 4/3$ than those in Fig. 10, with deviations from the 4 : 3 ratio not exceeding 1.5%.

When the calculation of Fig. 11 is repeated for concentrators having input acceptance angles $\theta_i = 50$, 70, and 80 deg, matched to the cone of signal radiation ($\theta_i = \theta_s$), the values of G_s and $G_s\overline{T}_s$ consistently scale in proportion to $\csc^2\theta_i$. Therefore, for a double CPC with $\theta_i = \theta_s < 90$ deg, the values of these two quantities can be obtained by scaling the values shown in Fig. 10 by a factor of $\csc^2\theta_i$. This simple scaling is expected to be valid only when the upper hollow CPC is a nearly ideal $\theta_i \rightarrow \theta_m$ transformer, which transfers radiation uniformly distributed within a large θ_i to radiation that is approximately uniform within a smaller θ_m. Our simulations verify that the upper hollow CPC of Fig. 2(c) is approximately an ideal $\theta_i \rightarrow \theta_m$ transformer. Moreover, extensive simulation shows that when the upper hollow CPC has a reflectance $\rho < 1$, the overall gain of the double-CPC concentrator is scaled by a factor ρ^{α}, where α, the average number of reflections, can be obtained from Fig. 9 (through simulation, this scaling is found to be accurate within 2%).

3.5 *Output Radiation Distribution and Antireflection Coating*

For infrared links operating in the near-infrared region of 800 to 1100 nm, the best photodetectors generally are silicon photodiodes, due to their low cost, low leakage current, and small capacitance per unit area. As the index of a dielectric CPC cannot generally be matched to the high index of silicon, to minimize reflection losses it is essential to apply an antireflection coating to the detector and to use index-matching

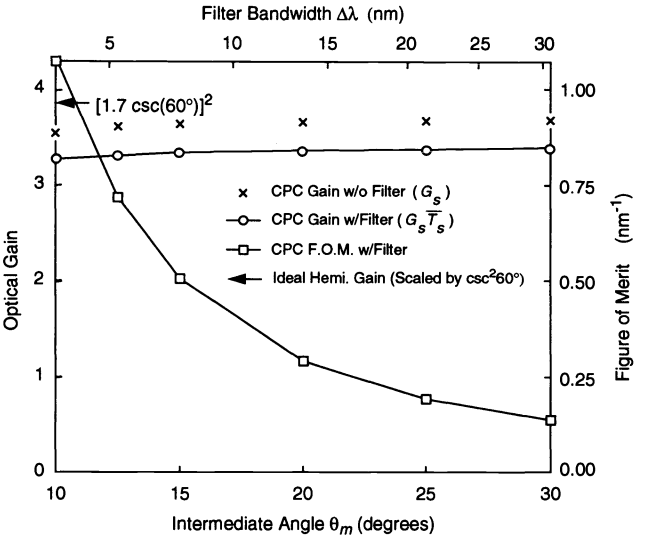

Fig. 11 Optical gain and figure of merit of a double CPC having input acceptance angle $\theta_i = 60$ deg, as a function of the intermediate angle θ_m (and, equivalently, the bandwidth $\Delta\lambda$ of the bandpass filter). The input signal radiation is distributed uniformly between 0 deg and $\theta_s = 60$ deg. The hollow CPC has a reflectance of 1, and the dielectric CPC has a refractive index of 1.7.

compound to achieve optical contact between the CPC and the detector (see Fig. 12).

As total reflection losses at the CPC-detector interface represent an average over all angles of incidence on the interface, it is necessary to know the angular distribution of radiation incident upon the interface. We expect this radiation to be isotropic, so that the power per unit solid angle exiting the CPC at angle θ with respect to the surface normal is proportional to $\cos\theta\, d\Omega \propto \cos\theta \sin\theta\, d\theta\, d\phi \propto \sin 2\theta\, d\theta$. To confirm that the radiation incident on the CPC-detector interface is isotropic, we have simulated the distribution of CPC output radiation for the three concentrators shown in Figs. 7, 10, and 11. As shown in Fig. 13, the simulated distributions are very nearly proportional to $\sin 2\theta$ for all three concentrators, and for dielectric CPC acceptance angles of both 10 and 20 deg. This $\sin 2\theta$ distribution is satisfied by the concentrators of Figs. 7, 10, and 11 because the filter angular bandwidth $\Delta\theta$ is matched to the acceptance angle of the dielectric CPC. By contrast, if we were to choose $\Delta\theta$ much smaller than the CPC acceptance angle and $\lambda_{\text{normal}} = \lambda_0$, all radiation exiting from the CPC would do so at nearly normal incidence.

Considering a signal wavelength near 800 nm, silicon has an index $n_s = 3.686$, while the index of typical dielectric concentrators ranges from about 1.4 to 1.8 (1.7 in our designs). A conventional antireflection coating for normal incidence would use a quarter-wave-thick layer having an index equal to the geometric mean of the CPC and detector indices (i.e., approximately 2.5). As we have isotropic incident radiation, we optimize numerically both the coating index and thickness, considering indices over the range from 1.8 to 2.7. Materials having indices in this range include TiO_x, Ta_2O_5, SiO_x, etc.[18] For coating indices in this range, Fig. 14 shows the coating thickness leading to minimum angle- and polarization-averaged reflectance, as well as the reflectance thereby achieved (coating thickness is normalized with respect to the quarter-wave optical thickness $\lambda/4n_a$, where n_a

Downloaded from SPIE Digital Library on 29 Sep 2010 to 171.64.84.32. Terms of Use: http://spiedl.org/terms

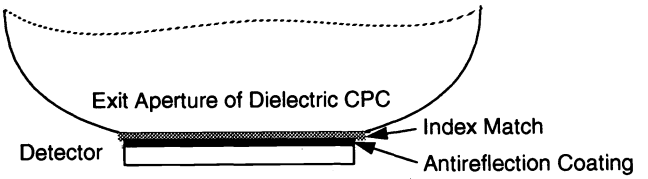

Fig. 12 At the transition between the dielectric CPC and the silicon detector, an index-matching compound (matched to the CPC) and an antireflection coating are used to ensure optical contact between the CPC and detector, thereby minimizing reflection losses.

is the coating index). If the antireflection coating material has a refractive index between 2.2 and 2.5, a reflectance as small as 4 to 5% can be achieved. The overall minimum reflectance is 4.3% for a $1.19(\lambda/4n_a)$-thick, index-2.39 coating (this range of indices can be achieved, e.g., by TiO_x). Without coating, the reflectance would be 18%. The coating thus provides an electrical SNR improvement of about 0.67 dB.

Silicon is absorptive at wavelength less than 1.1 μm, having[19] an absorption coefficient $\alpha = 10^3\ \mathrm{cm}^{-1}$ at wavelengths near 800 nm. Taking this absorption into account, the index has a complex value[14] $n_s = n - ik$, with $n = 3.686$ and $k = \alpha\lambda/4\pi = 0.006$. Figure 14 indicates the optimized coating thickness, and corresponding reflectance, calculated using the complex index. The optimized thickness is not observably affected, and the optimized reflectance is not reduced significantly.

4 Comparison of CPCs and Hemispherical Concentrators

In this section, we compare the dimensions of CPC- and hemisphere-based concentrators. To simplify the discussion, we assume that both types of concentrators are ideal. The nonideal properties of real CPCs were discussed in Sec. 3, and the nonidealities of real hemisphere-based concentrators have been described in recent publications.[4–7]

An idealized single CPC having index N and input acceptance angle $\theta_i \leq \theta_s$, when placed in a signal radiation flux limited to an angle θ_s, provides an optical gain of $N^2 \csc^2\theta_s$, independent of θ_i (see Sec. 2.1). Assuming that the CPC output aperture and detector have a radius r_c, such a CPC has an input aperture of radius[9] $r_i = r_c N \csc\theta_i$ and a length of

$$L = r_c(N \csc\theta_i + 1)(N^2 \csc^2\theta_i - 1)^{1/2} \ . \tag{20}$$

As described previously, such a concentrator is matched to a bandpass filter having angular bandwidth $\Delta\theta = \theta_i$. Substituting $\theta_i = \Delta\theta$ into Eq. (20) yields a relationship between the filter angular bandwidth and the concentrator length. A hemisphere of index N, when placed in the same signal radiation flux, provides an optical gain of N^2. If the hemisphere has radius R and it is coupled to a detector of radius r_h, then rays that reach the detector are incident on the hemisphere's outer surface at angles between 0 deg and $\theta_{\max}$, where[5,6] $\theta_{\max} = \sin^{-1}(r_h N/R)$. If a hemispherical filter having angular bandwidth $\Delta\theta$ is placed on this outer surface, then we must satisfy $\theta_{\max} = \Delta\theta$ to ensure that most of the signal passes through the filter. Accordingly, the hemisphere radius must not be smaller than

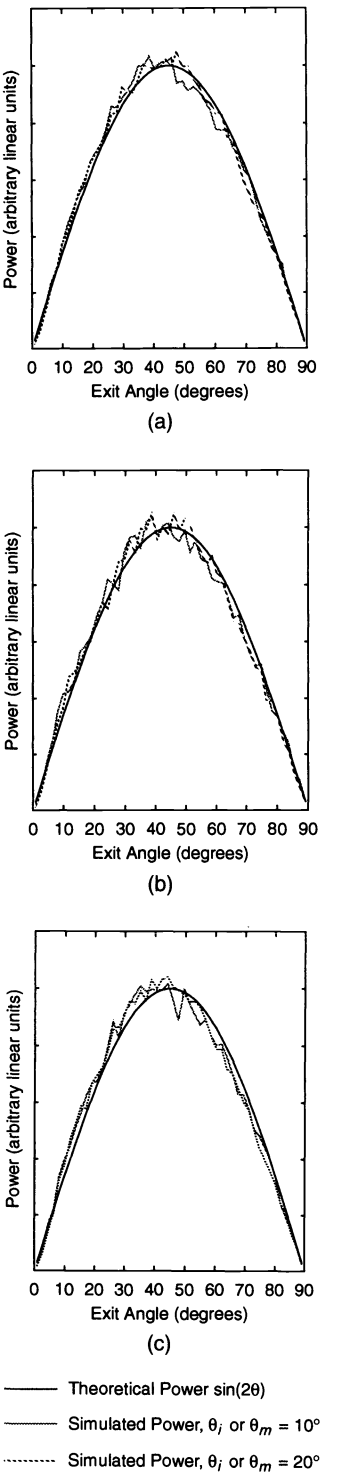

Fig. 13 Angular distribution of radiation at the exit aperture of dielectric CPCs: (a) design of Fig. 2(a) with $\theta_i = 10$, 20 deg; (b) design of Fig. 2(b) with $\theta_i = 90$ deg; $\theta_m = 10$, 20 deg; (c) design of Fig. 2(c) with $\theta_i = 60$ deg, $\theta_m = 10$, 20 deg.

$$R = r_h N \csc\Delta\theta \ . \tag{21}$$

In order that the hemisphere achieve a gain close to N^2, it is also necessary that $R \geq N^2 r_h$, but for the values of N and $\Delta\theta$ of interest here, this condition is less restrictive than Eq. (21).[4,6]

Downloaded from SPIE Digital Library on 29 Sep 2010 to 171.64.84.32. Terms of Use: http://spiedl.org/terms

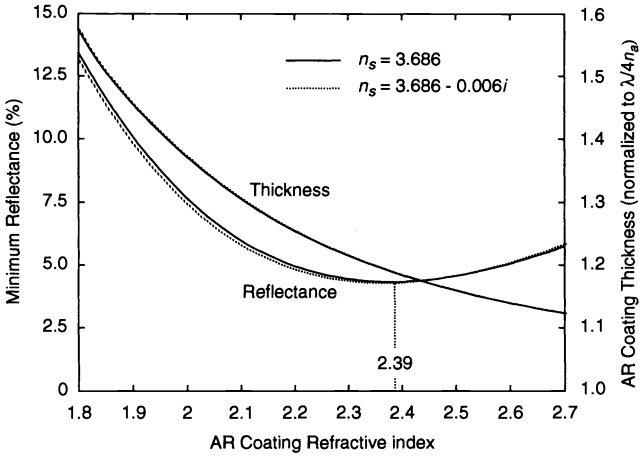

Fig. 14 Minimum angle- and polarization-averaged reflectance at dielectric-CPC–detector interface, as a function of the refractive index of the antireflection coating on the silicon detector. Also shown is the coating thickness leading to minimum reflectance. The CPC has a refractive index of 1.7, while the silicon detector has an index of 3.686 (a small imaginary part, corresponding to absorption, is also considered). Radiation incident on the interface is assumed to have a power per unit solid angle proportional to sin(2θ). If the coating material has refractive index between 2.2 and 2.5, the minimum reflectance can be as low as 4% to 5%.

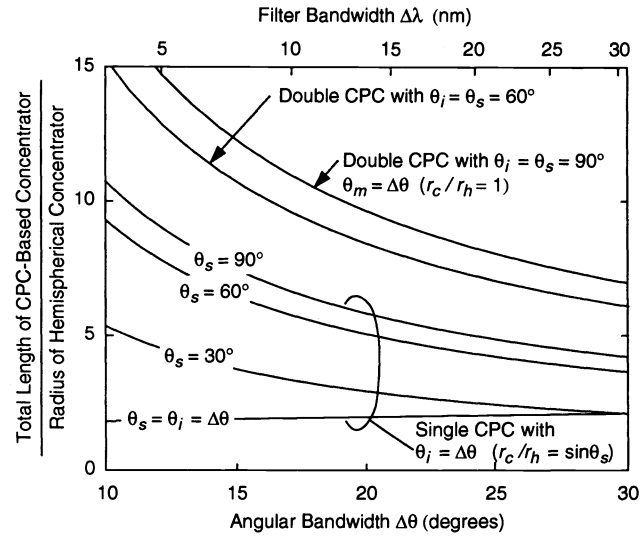

Fig. 15 Total length of single or double CPC as a function of the angular bandwidth Δθ (and, equivalently, the bandwidth Δλ of the bandpass filter). The length is normalized to the radius of a hemispherical filter-concentrator using a filter of the same bandwidth. The detector radii for the CPC (r_c) and for the hemisphere (r_h) are related as indicated, so that the CPC- and hemisphere-based receivers achieve the same electrical SNR. The dielectric CPCs and hemispheres have refractive indices of 1.7.

In order to compare the required dimensions of the CPC- and hemisphere-based concentrators, we assume that they share a common refractive index N and receive identical isotropic ambient radiation. Both concentrators present a gain of N^2 to this ambient. Both concentrators receive identical signal radiation, which is confined to a cone of angle θ_s. Both concentrators employ filters having an angular bandwidth $\Delta\theta$, and both receivers achieve the same electrical SNR. It is easily shown that the detector radii are related by $r_c = r_h \sin\theta_s$, i.e., when the signal radiation is restricted to an angle $\theta_s < 90$ deg, the CPC can employ a smaller detector than the hemisphere. The ratio of the length of the single CPC concentrator to the radius of the hemispherical concentrator is shown in Fig. 15 for $\theta_s = 30$, 60, and 90 deg, assuming $N = 1.7$. When the incident signal radiation is isotropic ($\theta_s = 90$ deg), the CPC length is much greater than the hemisphere radius, while when the signal radiation is confined to a narrower cone (e.g., $\theta_s = 30$ deg), the ratio of dimensions is more moderate. Figure 15 also illustrates the case when the signal radiation is confined to a narrow cone and the CPC input acceptance angle is matched to the signal radiation ($\theta_s = \theta_i = \Delta\theta$). Using Eqs. (20) and (21), it is easy to show that in the limit of small $\theta_s = \theta_i = \Delta\theta$, the length of the CPC is only $N + \sin\Delta\theta$ times larger than the radius of the hemisphere. Our results clearly indicate that to minimize the length of the CPC, its input acceptance angle should be matched to the cone of signal radiation.

An idealized double-CPC concentrator having an input acceptance angle $\theta_i \le \theta_s$ and a lower CPC of refractive index N, when placed in a cone of signal radiation confined to θ_s, can provide an optical gain of $N^2 \csc^2\theta_s$ (see Sec. 2.1). The considerations of that section show that the gain of such a double-CPC concentrator is independent of the refractive index of the upper CPC, and of the intermediate angle θ_m. As described in Sec. 2.4 the intermediate angle θ_m should be matched to the filter angular bandwidth $\Delta\theta$. The length of the lower dielectric CPC is thus given by (20), with the substitution of $\theta_m = \Delta\theta$ for θ_i. It is easy to show that the length of the upper hollow CPC is given by[9]

$$L' = r_c N(\csc\theta_m + \csc\theta_i)(N'^2 \csc^2\theta_m - 1)^{1/2} , \qquad (22)$$

where N' is the refractive index of the upper CPC and, as before, r_c is the detector radius. Clearly, the length of the upper CPC is minimized if we choose $N' = 1$, i.e., a hollow upper CPC. Since $\theta_i \le \theta_s$, the length of the upper CPC is also minimized if its input acceptance angle is matched to the cone of signal radiation, i.e., $\theta_i = \theta_s$. Assuming that the filter is matched to the lower CPC, we can substitute $\Delta\theta$ for θ_m in Eq. (22). In comparing the length of the double CPC with the radius of the hemisphere, we will assume $N' = 1$ and $\theta_i = \theta_s$. As before, we assume that the double CPC and hemisphere employ the same filter angular bandwidth $\Delta\theta$ and achieve the same electrical SNR, permitting us to set $r_c = r_h \sin\theta_s$. Figure 15 compares the overall length of the double-CPC concentrator ($L + L'$) with the radius of the hemisphere. We see that for a given θ_s, the double CPC is even longer than the single CPC, and has a length many times greater than the hemisphere radius.

While not pursuing it in detail here, we note that the use of truncated CPCs[9] is one means to reduce the length of the single- and double-CPC concentrators considered in this paper. In typical cases,[9] the CPC length can be reduced by half, with only a 16% reduction in concentration ratio.

5 Conclusions

We have discussed the design of CPC-based optical concentrators for use in wireless infrared communication systems. Unlike a hemispherical lens, which has a fixed optical gain

Downloaded from SPIE Digital Library on 29 Sep 2010 to 171.64.84.32. Terms of Use: http://spiedl.org/terms

of N^2 over a fixed FOV of 90 deg, CPC-based concentrators can achieve any FOV between 0 and 90 deg, and can achieve gains higher than N^2 when the FOV is less than 90 deg. While a narrowband hemispherical concentrator requires a hemispherical bandpass filter, which is difficult to fabricate, CPC-based concentrators utilize planar bandpass filters, which are easily fabricated. Three different concentrator designs, suitable for achieving various FOVs, have been analyzed both analytically and through numerical simulation. We have found that the optical gains of single and double CPCs are, respectively, about 94% and 93% those of ideal optical concentrators, while addition of planar bandpass filters decreases the gains to about 88% and 86%, respectively. Simulation also shows that the optical gain of a double CPC having overall input acceptance angle θ_i is approximately $\csc^2\theta_i$ times that of a double CPC having a 90-deg FOV. We have found that the radiation incident on the CPC exit aperture is isotropic, and have determined that an optimized single-layer antireflection coating can reduce the angle-averaged reflection losses at the CPC-detector interface to 4% to 5%. We have compared the physical dimensions of CPC-based and hemispherical concentrators that achieve equal receiver SNR. When the source is confined to a narrow range of angles, the length of a CPC is only about N times the radius of the hemisphere, where N is the refractive index of both concentrators. When the source subtends a wide field of view, however, the corresponding ratio of dimensions becomes very large.

Acknowledgments

The authors are grateful to Dr. Timothy Fohl for discussions that led us to undertake this study, and for valuable comments on an early draft of this manuscript. This work was supported by Siemens Corporation and National Science Foundation grant ECS-9408957.

References

1. F. R. Gfeller and U. H. Bapst, "Wireless in-house data communication via diffuse infrared radiation," *Proc. IEEE* **67**(11), 1474–1486 (1979).
2. M. D. Kotzin and A. P. van den Heuvel, "A duplex infra-red system for in-building communications," in *IEEE VTC '86,* pp. 179–185, 1986.
3. P. P. Smyth, M. McCullagh, D. Wisely, D. Wood, S. Ritchie, P. Eardley, and S. Cassidy, "Optical wireless local area networks—enabling technologies," *BT Technol. J.* **11**(2), 56–64 (1993).
4. J. R. Barry, *Wireless Infrared Communications,* Kluwer Academic, Boston, 1994.
5. J. M. Kahn, J. R. Barry, M. D. Audeh, J. B. Carruthers, W. J. Krause, and G. W. Marsh, "Non-directed infrared links for high-capacity wireless LANs," *IEEE Personal Commun. Mag.* **1**(2), 12–25 (1994).
6. J. R. Barry and J. M. Kahn, "Link design for nondirected wireless infrared communications," (in press).
7. J. P. Savicki and S. P. Morgan, "Hemispherical concentrators and spectral filters for planar sensors in diffuse radiation fields," *Appl. Opt.* **31**(34), 8057–8061 (1994).
8. G. Smestad, H. Ries, R. Winston, and E. Yablonovitch, "The thermodynamic limits of light concentrators," *Solar Energy Materials* **21**(2–3), 99–111 (1990).
9. W. T. Welford and R. Winston, *High Collection Nonimaging Optics,* Academic, New York (1989).
10. I. M. Bassett, W. T. Welford, and R. Winston, "Nonimaging optics for flux concentration," in *Progress in Optics,* E. Wolf, Ed., Vol. XXVII, pp. 161–226, North Holland, Amsterdam (1989).
11. J. D. Kuppenheimer, Jr., and P. F. Murphy, "Wide field of view–narrow band detection system," U.S. Patent No. 4,225,782 (1980).
12. M. C. Ruda, "How and when to use a nonimaging concentrator," in *International Conf. on Nonimaging Concentrators,* M. C. Ruda, Ed., *Proc. SPIE* **441,** 51–58 (1984).
13. D. R. Pauluzzi, P. R. McConnell, and R. L. Poulin, "Free-space undirected infrared voice and data communications with a comparison of RF systems," in *Proc. IEEE International Conf. on Selected Topics in Wireless Communication,* Vancouver, pp. 279–285 (1992).
14. H. A. Macleod, *Thin-Film Optical Filters,* 2nd ed., Chap. 7, p. 234, Adam Hilger, Bristol (1986).
15. H. A. Haus, *Waves and Fields in Optoelectronics,* Chap. 2, p. 42, Prentice-Hall, Englewood Cliffs, NJ (1985).
16. G. W. Marsh and J. M. Kahn, "50-Mb/s diffuse infrared free-space link using on-off keying with decision feedback equalization," *IEEE Photon. Technol. Lett.* **6**(10), 1268–1270 (1994).
17. J. M. Hammersley and D. C. Handscomb, *Monte Carlo Methods,* Chap. 5, p. 50, Chapman and Hall, London (1964).
18. A. Luque, *Solar Cells and Optics for Photovoltaic Concentration,* Chap. 14, p. 487, Adam Hilger, Bristol (1989).
19. S. M. Sze, *Physics of Semiconductor Devices,* Chap. 13, p. 750, Wiley, New York (1985).

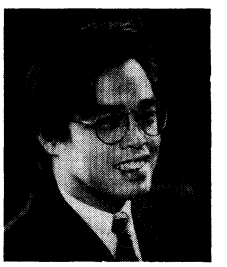

Keang-Po Ho received the BS degree in electrical engineering from National Taiwan University in 1991, and the MS degree in electrical engineering from the University of California at Berkeley in 1993. From 1992 to present, he is a research assistant in the Department of Electrical Engineering and Computer Sciences of the University of California at Berkeley, doing research in wireless and optical communication systems. He is expected to obtain his PhD degree in 1995. During the summer of 1994, he was working in IBM T. J. Watson Research Center on all-optical networks. His current research interests are wireless and optical communication systems, communication theory, multicarrier modulation, and crosstalk in dense wavelength division multiplexing systems.

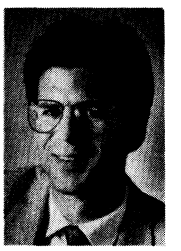

Joseph M. Kahn is an associate professor in the Department of Electrical Engineering and Computer Sciences at UC Berkeley. He received the AB in physics (1981), MA in physics (1983), and PhD in physics (1986) from UC Berkeley. His PhD thesis was entitled "Hydrogen-related acceptor complexes in germanium." From 1987 to 1990 he was a member of the technical staff in the Lightwave Communications Research Department of AT&T Bell Laboratories at Crawford Hill Laboratory in Holmdel, NJ, where he performed research on multigigabit-per-second coherent optical fiber transmission systems and related devices and subsystem technologies. He demonstrated the first BPSK-homodyne optical fiber transmission system, and achieved world records for receiver sensitivity in multigigabit-per-second systems. He joined the faculty of UC Berkeley in 1990, where his research interests include optical fiber communication networks and transmission systems, local-area networks using free-space optical links, and optical interconnects in digital systems. Dr. Kahn is a recipient of the National Science Foundation Presidential Young Investigator Award, and is a member of the IEEE Communications Society and IEEE Lasers and Electro-Optics Society. He is serving currently as a technical editor of *IEEE Personal Communications Magazine.*

Downloaded from SPIE Digital Library on 29 Sep 2010 to 171.64.84.32. Terms of Use: http://spiedl.org/terms